Crystallization of amorphous $Cu_{47}Ti_{34}Zr_{11}Ni_8$

S. C. Glade,[a] J. F. Löffler, S. Bossuyt, and W. L. Johnson
Division of Engineering and Applied Science, California Institute of Technology, Pasadena, California 91125

M. K. Miller
Microscopy and Microanalytical Sciences Group, Metals and Ceramics Division, Oak Ridge National Laboratory, P.O. Box 2008, Oak Ridge, Tennessee 37831-6136

(Received 21 August 2000; accepted for publication 17 October 2000)

The results of a study on the crystallization of amorphous $Cu_{47}Ti_{34}Zr_{11}Ni_8$ with the use of differential scanning calorimetry, transmission electron microscopy (TEM), x-ray diffraction, field ion microscopy, atom probe tomography (APT), and small-angle neutron scattering (SANS) are presented. These experimental techniques were used to characterize as-prepared samples and specimens heat treated at different temperatures around the glass transition temperature. APT and SANS show that the alloy decomposes into copper-enriched and titanium-enriched regions prior to nucleation and growth of a crystalline phase. TEM shows that the primary nucleating phase has a face centered cubic structure. © *2001 American Institute of Physics.* [DOI: 10.1063/1.1332089]

I. INTRODUCTION

In making metallic glasses, glass formation is equivalent to avoiding the nucleation and growth of crystalline phases when cooling the alloy from the molten liquid.[1] Hence, studies on the crystallization processes of metallic glass forming alloys are important to understanding glass formation in metallic systems; this knowledge will also aid in the development of better metallic glass forming alloys.

When metallic glasses crystallize at lower temperatures near the glass transition temperature, T_g, classical nucleation theory predicts few nuclei forming, resulting in a coarse microstructure. However, in many metallic glass forming alloys, including $Zr_{41.2}Ti_{13.8}Cu_{12.5}Ni_{10}Be_{22.5}$ (Refs. 2–4), $Mg_{62}Cu_{25}Y_{10}Li_3$ (Ref. 5), $Zr_{52.5}Cu_{17.9}Ni_{14.6}Al_{10}Ti_5$ (Ref. 6), and $Zr_{57}Cu_{15.4}Ni_{12.6}Al_{10}Nb_5$ (Ref. 6), a fine microstructure of nanocrystals embedded in an amorphous matrix is observed. Different models have been proposed to account for this observed microstructure.[7–10]

$Cu_{47}Ti_{34}Zr_{11}Ni_8$ is a glass forming alloy developed by Lin *et al.*,[11] with a critical cooling rate of ~250 K/s for glass formation. In this article, the results of a study on the crystallization of amorphous $Cu_{47}Ti_{34}Zr_{11}Ni_8$ are presented. $Cu_{47}Ti_{34}Zr_{11}Ni_8$ decomposes into copper-enriched and titanium-enriched regions before a crystalline phase nucleates and grows in the amorphous matrix. The primary nucleating phase has a face centered cubic structure.

II. EXPERIMENTAL METHODS

An alloy of nominal composition $Cu_{47}Ti_{34}Zr_{11}Ni_8$ was prepared from 99.9% to 99.9999% purity elemental metals in an arc melter with a titanium gettered, ultrahigh purity argon atmosphere. Ingots were flipped and melted repeatedly to promote homogeneity. To obtain amorphous samples, the alloy was remelted in a fused quartz tube in a high frequency induction furnace and then injection cast with ultrahigh purity argon into a copper mold.

Differential scanning calorimetry (DSC), performed with a Perkin Elmer DSC-7, was used to study the thermal behavior of $Cu_{47}Ti_{34}Zr_{11}Ni_8$. In isothermal experiments with the DSC, the amorphous solid was heated to different temperatures near the glass transition temperature and held isothermally. The DSC was calibrated at 0.0167 K/s for these experiments. DSC experiments at a heating rate of 0.333 K/s were also performed on samples of $Cu_{47}Ti_{34}Zr_{11}Ni_8$ that had been heat treated and isothermally annealed under various conditions. Isothermal anneals were performed by sealing a sample wrapped in tantalum foil in a quartz tube evacuated to a vacuum of 5×10^{-6} mbar or lower and placing this sample in an electric furnace.

Transmission electron microscopy (TEM) was performed on some of the heat treated and isothermally annealed samples with a Phillips EM430 operating at 300 kV with a lanthanum hexaboride electron source. All samples were prepared to electron transparency by ultramicrotomy.

Field ion microscopy (FIM) and atom probe tomography (APT) specimens were prepared by casting the alloy in a copper mold of dimensions $1\times4\times\sim25$ mm. Bars of cross section approximately 0.15 to 0.30 mm square were cut with a diamond saw. The bars were electropolished using 12.5% sulfuric acid in methanol (~9–14 V). Some bars were subsequently electropolished with a solution of 2% perchloric acid in 2-butoxyethanol (~9 V). Two different samples of $Cu_{47}Ti_{34}Zr_{11}Ni_8$ were characterized in the FIM/APT: as-prepared and isothermally annealed at 701 K for 24 h. The FIM/APT experiments were performed with an energy-compensated optical position-sensitive atom probe at Oak Ridge National Laboratory. Neon was used as the imaging gas for the FIM, with a sample temperature of 60 K. For the APT, the pulse fraction was 20% of the standing voltage and the pulse repetition rate was 1500 Hz.

[a]Author to whom all correspondence should be addressed; Electronic mail: sgladepm@hotmail.com

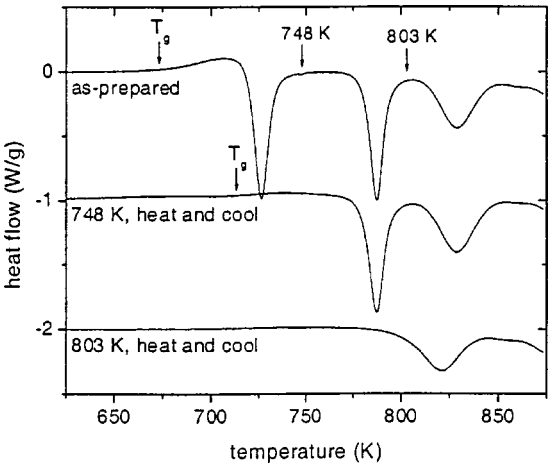

FIG. 1. Results from DSC scans performed at a heating rate of 0.333 K/s of as-prepared and heat treated $Cu_{47}Ti_{34}Zr_{11}Ni_8$ samples. The glass transition temperatures of the as-prepared ($T_g = 673$ K) and the 748 K heat treated ($T_g = 713$ K) samples are indicated.

Small-angle neutron scattering (SANS) experiments were performed at the intense pulsed neutron source at Argonne National Laboratory with the small-angle neutron diffractometer (SAND).[12] SANS data is taken in a Q region of 0.04 to 6 nm^{-1} ($Q = 4\pi \sin\theta/\lambda$, where θ is half the scattering angle and λ is the wavelength of the neutrons) in a single measurement using neutrons of wavelengths $\lambda = 0.1$ to 1.4 nm simultaneously in a time-of-flight mode. Samples for these experiments were prepared by injection casting $Cu_{47}Ti_{34}Zr_{11}Ni_8$ in a $1 \times 10 \times \sim 20$ mm copper mold. The samples were cut into pieces of cross section 10×10 mm and then isothermally annealed at 673, 683, 693, 708, and 723 K for 15 h and 743 K for 1 h in a vacuum furnace at a vacuum of 1×10^{-5} mbar. X-ray diffraction (XRD) was also performed on these specimens with a Scintag Pad V X-ray Powder Diffractometer with Cu K_α radiation on a θ–2θ goniometer equipped with a germanium solid state detector.

III. RESULTS

Figure 1 shows DSC scans of as-prepared and heat treated $Cu_{47}Ti_{34}Zr_{11}Ni_8$. When heating the as-prepared amorphous solid from room temperature, three exothermic peaks are observed (upper scan in Fig. 1). To observe the thermal behavior of the alloy after heating through these exotherms, two samples were heat treated by heating to 748 K and 803 K at 0.333 K/s and cooling at 3.33 K/s to room temperature. For both the 748 K and the 803 K heat treatments, the crystallization exotherms passed were not seen in subsequent DSC scans (lower scans in Fig. 1). The amorphous matrix of the sample heat treated at 748 K has a glass transition temperature, T_g, of 713 K, due to a shift in composition from the as-prepared state ($T_g = 673$ K).

A TEM dark field micrograph and electron diffraction pattern of the 748 K heat treated sample are shown in Fig. 2(a), revealing 2 to 3 nm nanocrystals in an amorphous matrix. Compared to the electron diffraction pattern from the as-prepared sample, the inner diffraction ring is sharper and the outer diffraction region is split due to the formation

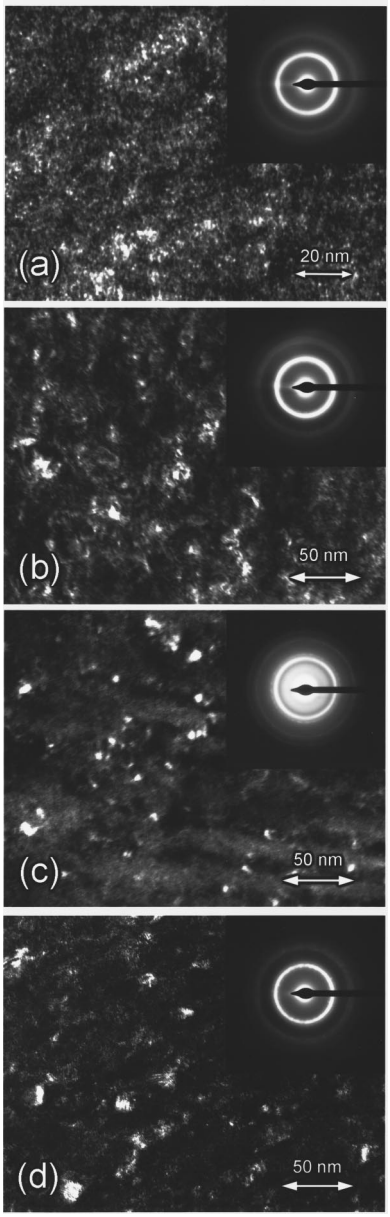

FIG. 2. Dark field TEM micrographs and electron diffraction patterns of $Cu_{47}Ti_{34}Zr_{11}Ni_8$ (a) heated up to 748 K at 0.333 K/s and cooled at 3.33 K/s, (b) heated up to 803 K at 0.333 K/s and cooled at 3.33 K/s, (c) isothermally annealed at 701 K for 24 h, and (d) isothermally annealed at 748 K for 3.5 h.

of these nanocrystals. This sharpening of the inner diffraction ring was also observed in annealed $Zr_{41.2}Ti_{13.8}Cu_{12.5}Ni_{10}Be_{22.5}$.[13] A TEM dark field micrograph and electron diffraction pattern of the 803 K heat treated sample are in Fig. 2(b), showing 5 nm and larger nanocrystals in an amorphous matrix. The phases in both samples could not be identified from the electron diffraction patterns.

To try to identify the primary nucleating phase in this alloy in the supercooled liquid temperature regime, isothermal anneals were performed at temperatures around the observed glass transition temperature of $Cu_{47}Ti_{34}Zr_{11}Ni_8$. A TEM dark field micrograph and electron diffraction pattern of a sample isothermally annealed at 701 K for 24 h are shown in Fig. 2(c). Nanocrystals of 5 nm in size in an amor-

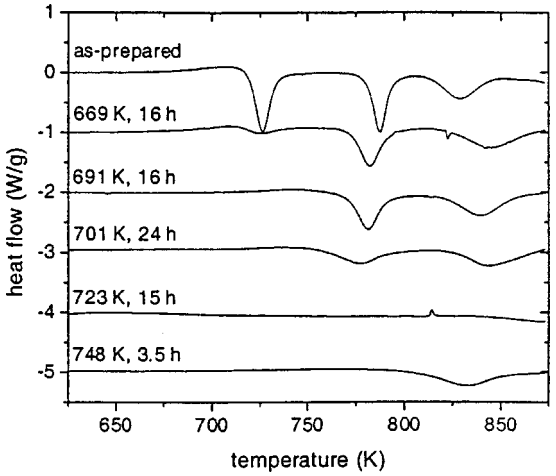

FIG. 3. DSC scans of as-prepared and isothermally annealed $Cu_{47}Ti_{34}Zr_{11}Ni_8$, performed at a heating rate of 0.333 K/s. The isothermal annealing conditions are indicated.

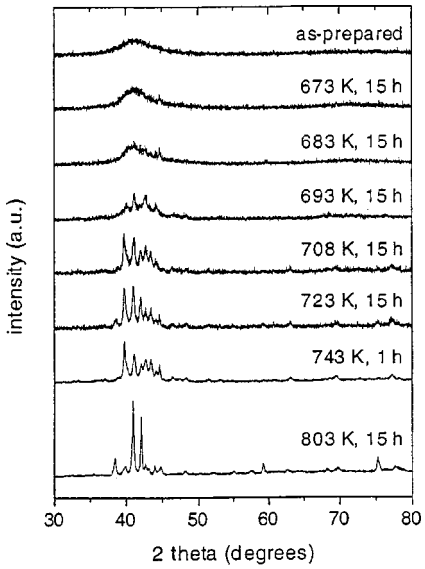

FIG. 4. XRD patterns of as-prepared and isothermally annealed $Cu_{47}Ti_{34}Zr_{11}Ni_8$. The scans performed on the 743 K, 1 h and the 803 K, 15 h isothermally annealed samples have improved signal to noise ratios due to longer scanning times. The isothermal annealing conditions are indicated.

phous matrix are observed. The nanocrystals have been identified as a face centered cubic phase with lattice parameter $a=3.8$ Å. Figure 3 includes a DSC scan of this sample; the first exotherm in the DSC scan is not present, and the remaining exotherms are broader than in the as-prepared sample (first scan in Fig. 3). The other DSC scans of isothermally annealed $Cu_{47}Ti_{34}Zr_{11}Ni_8$ shown in Fig. 3 will be discussed in conjunction with the further TEM and XRD results.

To try to identify the phase in the 748 K heat treated sample, a sample was isothermally annealed at 748 K for 3.5 h. A TEM dark field micrograph and electron diffraction pattern of this sample are shown in Fig. 2(d). Nanocrystals of an average size of 5 to 10 nm in an amorphous matrix are observed. The phases in this sample could not be identified in the electron diffraction pattern. However, similar phases are nucleating and growing in this sample and in the sample heat treated at 803 K, as evidenced by the diffraction patterns [Figs. 2(b) and 2(d)]. After the isothermal anneal at 748 K for 3.5 h, the first and second exothermic peaks are not present in the DSC scan (as shown in the lowest scan in Fig. 3).

A sample isothermally annealed at 691 K for 16 h and observed in the TEM (micrograph not shown) showed 1 nm nanocrystals forming. A DSC scan of this sample, included in Fig 3, shows that the first crystallization exotherm is not present, while the second and third crystallization exotherms can still be observed.

XRD patterns of $Cu_{47}Ti_{34}Zr_{11}Ni_8$, as-prepared and isothermally annealed, are shown in Fig. 4. The samples isothermally annealed at 673, 683, and 693 K for 15 h exhibit small peaks on the broad amorphous hump, due to nanocrystals forming in the amorphous matrix. The samples isothermally annealed at 708, 723, and 803 K for 15 h and 743 K for 1 h show further evidence of crystallization, with the amorphous background diminishing and the crystalline peaks becoming more intense. A DSC scan of the sample annealed at 723 K for 15 h (Fig. 3) shows no crystallization exotherms, giving evidence that the sample has a high crystalline volume fraction.

Field ion micrographs of $Cu_{47}Ti_{34}Zr_{11}Ni_8$, as-prepared and isothermally annealed at 701 K for 24 h, are shown in Fig. 5. FIM of the as-prepared $Cu_{47}Ti_{34}Zr_{11}Ni_8$ revealed no ring patterns (poles), which result from a crystalline structure. The isothermally annealed $Cu_{47}Ti_{34}Zr_{11}Ni_8$ revealed nanocrystals in an amorphous matrix, as also evidenced by TEM. The composition of one nanocrystal was measured as 79.31 ± 1.06 at. % Ti, 19.20 ± 1.03 at. % Zr, 0.14 ± 0.10 at. % Cu, and 0.34 ± 0.15 at. % Ni.

For analysis of APT data, the three-dimensional map of atoms collected from a cylinder of material in the specimen is divided into small blocks of atoms (100 atoms per block) and a frequency distribution of the composition of each atomic species in each individual block is constructed. To determine if decomposition has occurred, these frequency distributions are compared to the frequency distribution expected from a random distribution of atoms in an alloy of the same mean composition. Frequency distributions generated by different models of decomposition are then generated and fit to the experimentally measured frequency distribution; pa-

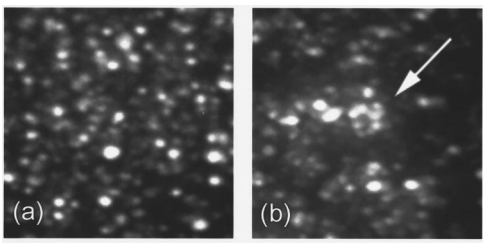

FIG. 5. Field ion microscope image of (a) as-prepared and (b) isothermally annealed (at 701 K for 24 h) $Cu_{47}Ti_{34}Zr_{11}Ni_8$. The arrow in (b) highlights a nanocrystal.

TABLE I. Results of the statistical analysis of $Cu_{47}Ti_{34}Zr_{11}Ni_8$ APT data using the P_a model. The parameters P_a and Δc are given in atomic fraction. Bold entries in the χ^2 column indicate the fit is rejected at the 95% level.

As-prepared	P_a	Standard error	χ^2	Degrees of freedom	$\Delta c = 2P_a$
Cu	0.068	0.008	18.0	24	0.136
Ti	0.056	0.008	20.2	23	0.112
Zr	0.000		3.9	13	0.000
Ni	0.007	0.006	8.4	10	0.014
Isothermally annealed at 701 K for 24 h.					
	P_a	Standard error	χ^2	Degrees of freedom	$\Delta c = 2P_a$
Cu	0.108	0.004	**217.6**	39	0.216
Ti	0.108	0.005	**345.1**	40	0.216
Zr	0.028	0.002	15.9	19	0.056
Ni	0.019	0.001	9.8	14	0.058
Isothermally annealed at 701 K for 24 h.					
	P_a	Standard error	χ^2	Degrees of freedom	$\Delta c = 2P_a$
Cu	0.073	0.007	21.0	26	0.146
Ti	0.056	0.007	20.3	24	0.112
Zr	0.021	0.004	6.7	15	0.042
Ni	0.032	0.002	**29.2**	15	0.064

rameters contained in these models can then be compared, giving a measure of the composition differences in decomposed regions.

The two models used to generate probability distributions for a decomposed sample in this investigation were the sinusoidal or P_a model[14] and the Langer, Bar-on, and Miller (LBM) model.[15] The P_a model considers decomposition to occur spinodally and is based on a sinusoidal variation in composition. The P_a model considers different samples from a discretized composition profile

$$p_j = P_0 + P_a \sin\left[\frac{2\pi j}{n_d}\right], \quad \{j: 0 \leqslant j \leqslant n_d\}, \tag{1}$$

where $2P_a$ is the peak-to-peak amplitude of the spinodal, P_0 is the mean composition, and n_d is the discretization, i.e., a number chosen to ensure that the estimate is independent of n_d ($n_d = 20$, in our calculations). The maximum likelihood estimates of composition amplitudes are then calculated. The P_a model has one independent parameter, P_a. The difference in the composition of the two decomposed phases is given by $\Delta c = 2P_a$. The results of the statistical analysis with the P_a model are listed in Table I for the data sets collected (one as-prepared sample and two isothermally annealed samples). The standard error is the error in the P_a value, and the χ^2 and the degrees of freedom values are used to determine the confidence level of the fit.

$Cu_{47}Ti_{34}Zr_{11}Ni_8$ exhibits decomposition primarily through the partitioning of copper and titanium in both the as-prepared and isothermally annealed states, as evidenced by the Δc values. In one of the isothermally annealed specimens, the degree of decomposition is more than in the as-prepared state. In the other isothermally annealed specimen, the degree of decomposition is of the same magnitude as in the as-prepared sample. This difference is probably due to regional variations and possibly due to the FIM/APT specimens being taken from different areas of the 1 mm thick strip of the bulk material. Further analysis of the data with contingency tables showed that the copper and titanium are antisegregated; i.e., the copper-enriched regions are low in titanium and vice versa.

The LBM model considers nonlinear spinodal decomposition using a double Gaussian distribution with the probability distribution function

$$P(c) = \frac{\mu_2 \exp\left[\frac{-(c-\mu_1)^2}{2\sigma^2}\right] + \mu_1 \exp\left[\frac{-(c-\mu_2)^2}{2\sigma^2}\right]}{(\mu_1+\mu_2)\sigma\sqrt{2\pi}}. \tag{2}$$

One Gaussian is centered at μ_1, the other is center at μ_2, and both have a width σ. The LBM model has three independent parameters, μ_1, μ_2, and σ. In implementations of the LBM model, the two parameters $b_1 = c - \mu_1$ and $b_2 = \mu_2 - c$, where c is the mean concentration, are substituted into Eq. (2). The difference in the composition of the two decomposed phases is given by $\Delta c = b_1 + b_2$. The results of the statistical analysis with the LBM model are listed in Table II for the data sets collected. As in the P_a model, the Δc values in the LBM model show that the alloy primarily decomposes to copper-enriched and titanium-enriched regions. Further details on both the P_a and the LBM models can be found in Refs. 16 and 17.

Data from the SANS experiments, scattering cross section $S(Q)$ versus scattering vector Q, are shown in Fig. 6. The as-prepared and the isothermally annealed at 673 K for 15 h samples exhibit no scattering signal, i.e., these samples have no detectable composition fluctuations in a size regime of 1 to 150 nm. The samples isothermally annealed at higher temperatures all exhibit interference peaks, giving evidence of scattering inhomogeneities. In these higher temperature annealed samples, the inhomogeneities are nanocrystals in the amorphous matrix, as shown by TEM. The intensity of the interference peaks increase with increasing temperature, due to the increase in the volume fraction of the scattering nanocrystals.

After the sample was held for a period of time at an elevated temperature during isothermal DSC experiments, a broad exothermic heat release, on the order of 1 kJ g-atom^{-1}, was observed. This heat release is due to the formation of nanocrystals. An Arrhenius plot, with the points indicating the onset of the heat release, is shown in Fig. 7. The onset of the heat release follows an Arrhenius law,

$$\frac{1}{t} \propto \exp\left(\frac{-E}{k_B T}\right), \tag{3}$$

where t is time (in seconds). The activation energy is $E = 4.28(\pm 0.11)$ eV, obtained by a fit to the data.

IV. DISCUSSION

$Zr_{41.2}Ti_{13.8}Cu_{12.5}Ni_{10}Be_{22.5}$, with a critical cooling rate of 1 K/s for glass formation,[18] is one of the best metallic glass formers yet developed. The thermophysical properties of $Zr_{41.2}Ti_{13.8}Cu_{12.5}Ni_{10}Be_{22.5}$ have been well characterized,

TABLE II. Results of the statistical analysis of $Cu_{47}Ti_{34}Zr_{11}Ni_8$ APT data using the LBM model. The parameters b_1, b_2, σ, and Δc are given in atomic fraction.

As-prepared	$b1$	$b2$	σ	χ^2	Degrees of freedom	$\Delta c = b_1 + b_2$
Cu	0.040	0.050	0.020	16.870	24	0.090
Ti	0.050	0.030	0.010	19.313	23	0.080
Zr	0.010	0.010	0.010	8.842	14	0.020
Ni	0.010	0.010	0.010	11.997	11	0.020
Isothermally annealed at 701 K for 24 h.						
	$b1$	$b2$	σ	χ^2	Degrees of freedom	$\Delta c = b_1 + b_2$
Cu	0.100	0.030	0.060	39.114	42	0.130
Ti	0.010	0.160	0.070	43.979	45	0.170
Zr	0.010	0.030	0.010	19.531	20	0.050
Ni	0.010	0.010	0.010	8.782	14	0.020
Isothermally annealed at 701 K for 24 h.						
	$b1$	$b2$	σ	χ^2	Degrees of freedom	$\Delta c = b_1 + b_2$
Cu	0.020	0.070	0.040	17.918	27	0.090
Ti	0.050	0.030	0.010	18.842	24	0.080
Zr	0.010	0.020	0.010	6.254	15	0.030
Ni	0.070	0.010	0.010	10.407	15	0.080

including its crystallization behavior. Crystallization at lower temperatures (achieved by isothermally annealing samples near the glass transition temperature) proceeds by the alloy decomposing into titanium-enriched regions,[3,4] followed by the polymorphic nucleation of metastable face centered cubic Cu–Ti nanocrystals ($a = 4.0$ Å). *In situ* SANS experiments support the idea that a chemical decomposition on the nanometer scale with titanium involved initiates an abrupt onset of nucleation, resulting in a microstructure of nanocrystals in an amorphous matrix.[10]

The crystallization of the $Cu_{47}Ti_{34}Zr_{11}Ni_8$ glass forming alloy shows similarities to that of $Zr_{41.2}Ti_{13.8}Cu_{12.5}Ni_{10}Be_{22.5}$. Decomposition into copper-enriched and titanium-enriched regions was observed in the as-prepared and isothermally annealed states; regions high in copper content are low in titanium content and vice versa. Face centered cubic nanocrystals, with a lattice parameter of $a = 3.8$ Å, nucleated and grew in the amorphous matrix. The composition of one nanocrystal was determined by APT in a sample annealed isothermally at 701 K for 24 h. This nanocrystal contained about 80% titanium and 20% zirconium. However, this does not exclude nanocrystals of other compositions forming.

According to the titanium–zirconium phase diagram,[19] titanium and zirconium form a hexagonal close packed solid solution at all compositions. Face centered cubic titanium and zirconium phases can be formed at high pressures at 700

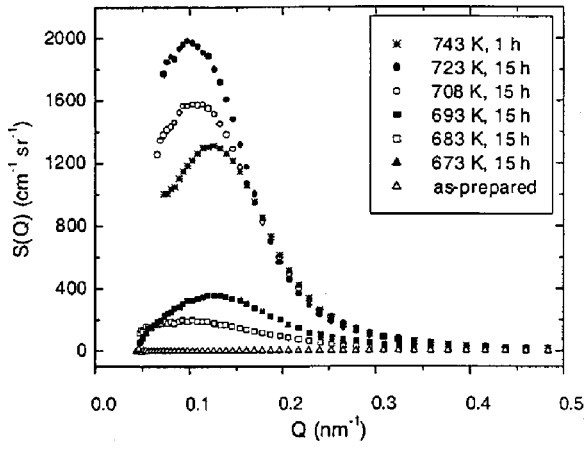

FIG. 6. SANS data from an as-prepared amorphous sample of $Cu_{47}Ti_{34}Zr_{11}Ni_8$ and $Cu_{47}Ti_{34}Zr_{11}Ni_8$ samples isothermally annealed at various temperatures and times, as indicated in the legend. The data from the as-prepared and the 673 K, 15 h isothermally annealed samples lie on top of each other.

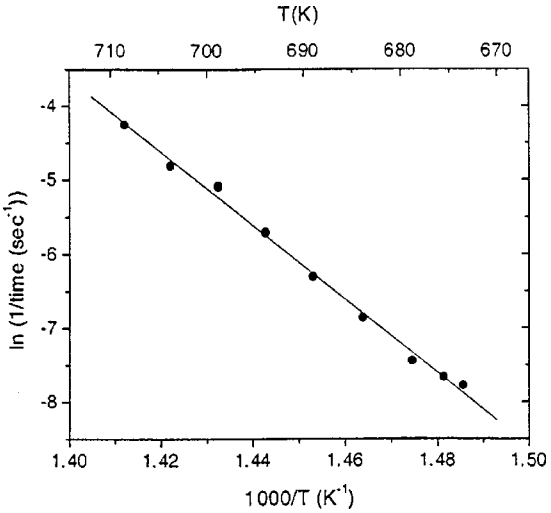

FIG. 7. Arrhenius plot of data obtained from isothermal anneals of $Cu_{47}Ti_{34}Zr_{11}Ni_8$. Points indicate the time when heat (~1 kJ g-atom^{-1}) was released from the sample during the isothermal anneal.

K (the temperature of our heat treatments), but the free energy of formation of these face centered cubic phases is ~250 kJ/mol.[20] Therefore, it is unlikely that the titanium–zirconium nanocrystal detected in FIM/APT corresponds to the face centered cubic phase detected in TEM.

The microstructure of the beams analyzed in the atom probe represents the state of the alloy when it is cooled from the melt at ~4000 K/s by casting the alloy in 1 mm thick strips; simple arguments relate the thickness of the cast sample to the cooling rate.[11] From the P_a and LBM models, decomposition is already present in a sample cooled at this rate. The isothermal anneals increased the magnitude of decomposition, as seen in the Δc values for each alloy.

Previous work by Miller *et al.*[21] on as-prepared $Cu_{47}Ti_{34}Zr_{11}Ni_8$ revealed solute clustering, with antisegregation of copper and titanium, as well as nanocrystals in an amorphous matrix. No nanocrystals were observed in the as-prepared $Cu_{47}Ti_{34}Zr_{11}Ni_8$ samples in this study. The samples Miller *et al.*[21] used were prepared with a lower cooling rate of ~1000 K/s (by casting the alloy in 2 mm thick strips), which presumably allowed enough time for the nucleation of nanocrystals.

The fact that $Cu_{47}Ti_{34}Zr_{11}Ni_8$ decomposes and nanocrystals form is also supported by the SANS measurements, which show an interference maximum for the isothermally annealed samples. The SANS intensity, however, is one to two orders of magnitude higher than that in similar experiments performed on annealed $Zr_{41.2}Ti_{13.8}Cu_{12.5}Ni_{10}Be_{22.5}$ (Refs. 8 and 10) and $Zr_{52.5}Cu_{17.9}Ni_{14.6}Al_{10}Ti_5$.[6] This is due to the greater amount of titanium, which has a negative scattering length, present in $Cu_{47}Ti_{34}Zr_{11}Ni_8$. The scattering intensity of the samples annealed for 15 h at 708 and 723 K is larger than that of the sample annealed for 1 h at 743 K. Thus, nanocrystallization is not complete after 1 h of annealing, even at a temperature of 70 K above T_g. This is in agreement with the DSC scans of Fig. 3, where an exothermic peak is still visible after 3.5 h annealing at 748 K, but no peak is observed after 15 h annealing at 723 K. One possibility is that the nucleation rate at similar temperatures above T_g (i.e., $T-T_g$) is much lower in $Cu_{47}Ti_{34}Zr_{11}Ni_8$ than in $Zr_{41.2}Ti_{13.8}Cu_{12.5}Ni_{10}Be_{22.5}$ and $Zr_{52.5}Cu_{17.9}Ni_{14.6}Al_{10}Ti_5$.

Furthermore, in contrast to observations on $Zr_{41.2}Ti_{13.8}Cu_{12.5}Ni_{10}Be_{22.5}$ and $Zr_{52.5}Cu_{17.9}Ni_{14.6}Al_{10}Ti_5$, the Q values of the interference peaks, $Q_{\max}$, do not systematically shift to lower values with increasing annealing temperature in $Cu_{47}Ti_{34}Zr_{11}Ni_8$, as is expected with a mechanism of spinodal decomposition.[22] The interference maximum, $Q_{\max}$, is about 0.1 nm^{-1} in $Cu_{47}Ti_{34}Zr_{11}Ni_8$; $Q_{\max}$ shifts from 0.4 to 0.1 nm^{-1} in $Zr_{41.2}Ti_{13.8}Cu_{12.5}Ni_{10}Be_{22.5}$, and from 0.3 to 0.2 nm^{-1} in $Zr_{52.5}Cu_{17.9}Ni_{14.6}Al_{10}Ti_5$, for similar annealing temperatures above T_g. Although TEM shows similar results for $Zr_{41.2}Ti_{13.8}Cu_{12.5}Ni_{10}Be_{22.5}$ and $Cu_{47}Ti_{34}Zr_{11}Ni_8$, the crystallization process of $Cu_{47}Ti_{34}Zr_{11}Ni_8$ may differ from that in zirconium based alloys. Additional *in situ* small-angle x-ray scattering experiments have been performed on $Cu_{47}Ti_{34}Zr_{11}Ni_8$ to further investigate this crystallization process.[23]

The onset of nucleation data from the isothermal DSC experiments follows an Arrhenius law. The activation energy calculated, $E=4.28(\pm 0.11)$ eV, is comparable to the value attributed to titanium diffusion in $Zr_{41.2}Ti_{13.8}Cu_{12.5}Ni_{10}Be_{22.5}$ [$E=4.09(\pm 0.76)$ eV].[10,24] This suggests that the nucleation of nanocrystals in $Cu_{47}Ti_{34}Zr_{11}Ni_8$ is a diffusion controlled process.

V. SUMMARY

Different experimental techniques were used to investigate the crystallization of amorphous $Cu_{47}Ti_{34}Zr_{11}Ni_8$. Similar to other metallic glass forming alloys, $Cu_{47}Ti_{34}Zr_{11}Ni_8$ decomposes prior to crystallization. $Cu_{47}Ti_{34}Zr_{11}Ni_8$ decomposes into copper-enriched and titanium-enriched regions (the copper-enriched regions are low in titanium content and vice versa). The primary nucleating phase has a face centered cubic structure.

ACKNOWLEDGMENTS

The authors thank C. M. Garland for assistance with the TEM work and K. F. Russell for assistance with the FIM/APT experiments. The SANS measurements were performed with P. Thiyagarajan at Argonne National Laboratory. This work was supported by the U.S. Department of Energy (Grant No. DEFG-03-86ER45242), NASA (Grant No. NAG8-1744) (W.J.) and the Alexander von Humboldt Foundation via the Feodor Lynen Program (J. L.). Research at the Oak Ridge National Laboratory SHaRE User Facility was sponsored by the Division of Materials Sciences and Engineering, U.S. Department of Energy, under Contract No. DE-AC05-00OR22725 with UT-Battelle, LLC, and through the SHaRE Program under Contract No. DE-AC05-76OR00033 with Oak Ridge Associated Universities.

[1] A. L. Greer, Science **267**, 1947 (1995).
[2] A. Peker and W. L. Johnson, Appl. Phys. Lett. **63**, 2342 (1993).
[3] S. Schneider, P. Thiyagarajan, and W. L. Johnson, Appl. Phys. Lett. **68**, 493 (1996).
[4] M. P. Macht, N. Wanderka, A. Wiedenmann, H. Wollenberger, Q. Wei, H. J. Fecht, and S. G. Close, Mater. Sci. Forum **225**, 65 (1996).
[5] W. Liu and W. L. Johnson, J. Mater. Res. **11**, 2388 (1996).
[6] J. F. Löffler, S. Bossuyt, S. C. Glade, W. L. Johnson, W. Wagner, and P. Thiyagarajan, Appl. Phys. Lett. **77**, 525 (2000).
[7] M. Calin and U. Köster, Mater. Sci. Forum **269**, 749 (1998).
[8] S. Schneider, P. Thiyagarajan, U. Geyer, and W. L. Johnson, Physica B **241**, 918 (1998).
[9] K. F. Kelton, Philos. Mag. Lett. **77**, 337 (1998).
[10] J. F. Löffler and W. L. Johnson, Appl. Phys. Lett. **76**, 3394 (2000).
[11] X. H. Lin and W. L. Johnson, J. Appl. Phys. **78**, 6514 (1995).
[12] P. Thiyagarajan, J. E. Epperson, R. K. Crawford, J. M. Carpenter, T. E. Klippert, and D. G. Wozniak, J. Appl. Crystallogr. **30**, 280 (1997).
[13] S. Schneider, U. Geyer, P. Thiyagarajan, R. Busch, R. Schulz, K. Samwer, and W. L. Johnson, Mater. Sci. Forum **225**, 59 (1996).
[14] J. M. Sassen, M. G. Hetherington, T. J. Godfrey, G. D. W. Smith, P. H. Pumphrey, and K. N. Akhurst in *Properties of Stainless Steels in Elevated Temperature Service*, edited by M. Prager (American Society of Mechanical Engineers, New York, 1987), p. 65.
[15] J. S. Langer, M. Bar-on, and H. D. Miller, Phys. Rev. A **11**, 1417 (1975).
[16] M. K. Miller, A. Cerezo, M. G. Hetherington, and G. D. W. Smith, *Atom Probe Field Ion Microscopy* (Oxford University Press, Oxford, 1996).
[17] M. K. Miller, K. O. Bowman, A. Cerezo, and J. M. Hyde, Appl. Surf. Sci. **67**, 429 (1993).

[18] Y. J. Kim, R. Busch, W. L. Johnson, A. J. Rullison, and W. K. Rhim, Appl. Phys. Lett. **65**, 2136 (1994).
[19] *Binary Alloy Phase Diagrams*, edited by T. B. Massalski, 2nd. ed. (American Society for Metals, Metals Park, Ohio, 1990).
[20] Thermodynamic data from TAPP database, version 2.2, E S Micoware, Inc., Hamilton, OH (1994).
[21] M. K. Miller, K. F. Russell, P. M. Martin, R. Busch, and W. L. Johnson, J. Phys. IV **6**, 217 (1996).
[22] E. L. Huston, J. W. Cahn, and J. E. Hillard, Acta Metall. **14**, 1053 (1966).
[23] S. Bossuyt, J. F. Löffler, S. C. Glade, W. L. Johnson, S. Seifert, and P. Thiyagarajan (unpublished).
[24] E. Budke, P. Felitz, M. P. Macht, V. Naundorf, and G. Frohberg, Defect Diffus. Forum **143**, 825 (1997).